Draft of 2018.09.16–23:30

MNRAS **000**, 1–7 (0000) Preprint 16 September 2018 Compiled using MNRAS LATEX style file v3.0

The Second LBA Calibrator Survey of southern compact extragalactic radio sources — LCS2

Leonid Petrov[1⋆], Alet de Witt[2], Alessandra Bertarini[3], Elaine M. Sadler[4], Chris Phillips[5], and Shinji Horiuchi[6],

[1] *NASA, Goddard Space Flight Center, 8801 Greenbelt Rd, MD 22071, USA*
[2] *Hartebeesthoek Radio Astronomy Observatory, P.O.Box 443, Krugersdorp 1740, South Africa*
[3] *Institute of Geodesy and Geoinformation, University of Bonn, Nussallee 17, Bonn, Germany and Max Planck Institute for Radioastronomy, Bonn, Germany*
[4] *Sydney Institute for Astronomy, School of Physics, The University of Sydney, NSW 2006, Australia*
[6] *CSIRO Astronomy and Space Science, PO Box 76, Epping, NSW 1710, Australia*
[7] *Shinji's affiliation, Australia*

Accepted XXX; Received YYY; in original form ZZZ

ABSTRACT

We present the second catalogue of accurate positions and correlated flux densities for 1100 compact extragalactic radio sources that were not observed before 2008 at high resolution. The catalogue spans the declination range $[-90°, -30°]$ and was constructed from eitheen 24-hour VLBI observing sessions with the Australian Long Baseline Array at 8.3 GHz. The catalogue presents the final part of the program that was started in the 2008. The goals of that campaign are 1) to extend the number of compact radio sources with precise coordinates and measured correlated flux densities, which can be used for phase referencing observations, geodetic VLBI, search for sources with significant offset with respect to *Gaia* positions, and space navigation; 2) to extend the complete flux-limited sample of compact extragalactic sources to the southern hemisphere; and 3) to investigate the parsec-scale properties of sources from the high-frequency AT20G survey. The median uncertainty of the source positions is 3.5 mas. As a result of this VLBI campaign, the number of compact radio sources south of declination $-40°$ which have measured VLBI correlated flux densities and positions known to milliarcsecond accuracy has increased by a factor of 6.4. The catalogue and supporting material is available at `http://astrogeo.org/lcs`.

Key words: astrometry – catalogues – instrumentation: interferometers – radio continuum – surveys

1 INTRODUCTION

Until recently, the method of very long baseline interferometry (VLBI) proposed by Matveenko et al. (1965) was the only way to measure positions of extragalactic radio sources that are almost exclusively active galactic nuclea (AGNs) with sub-nanoradian accuracy. Recently, it has been demonstrated (Lindegren et al. 2016) that *Gaia* is able to get the position accuracy in par with VLBI. However, comparison of VLBI and *Gaia* matching sources showed (Mignard et al. 2016; Petrov & Kovalev 2017b) that there is a population of sources with statistically significant position offsets. A more detailed analysis by Kovalev et al. (2017) revealed that VLBI/*Gaia* offsets have a preferred direction along the jet with the mean offset in a range of 1–2 mas that was interpreted as a manifestation of the contribution of optical jet to the centroid position. This allowed Petrov & Kovalev (2017a) to make a conclusion that VLBI/*Gaia* difference is due to the fact VLBI and *Gaia* see different part of a source and further improvement in accuracy beyond 1–2 mas level will not result in a reconciliation of VLBI and *Gaia* coordinates of active galaxies. Moreover, the VLBI/*Gaia* offsets brings an important signal that allows us to make an inference about milliarcsecond scale source structure of AGNs that currently cannot be observed directly. As a consequence, if we need achieve accuracy better 1–2 mas, we

⋆ E-mail:Leonid.Petrov@nasa.gov

cannot borrow *Gaia* positions of a matching sources, but have to rely on VLBI determination of source coordinates for applications that needs high accuracy, such as space navigation, Earth orientation parameter monitoring, and comparison of positions of pulsars determined with VLBI and timing.

In this context, it becomes increasingly important to have an all-sky, deep, and precise catalogue of positions of extragalactic sources from radio observations. The most productive instrument for absolute radio astrometry is the Very Long Baseline Array. Using VLBA, one can easily determine positions of sources at declinations [-30°, +90°] (Beasley et al. 2002; Petrov et al. 2005, 2006; Kovalev et al. 2007; Petrov et al. 2008; Petrov 2011, 2013; Petrov & Taylor 2011; Petrov et al. 2011a; Immer et al. 2011; Condon et al. 2016; Gordon et al. 2016; Petrov 2016); with some difficulties positions of sources at declinations [-45°, -30°] (Fomalont et al. 2003); but with some exceptions one cannot observe sources below -45°. The sequence of VLBA Calibrator Surveys 1–9 (VCS) (e.g., Petrov et al. 2008, and references therein) provided a dense grid of calibrator sources.

The lack of a VLBA analogue in the southern hemisphere resulted in the past in a significant hemisphere disparity of the source distribution in absolute radioastrometry catalogues. To alleviate this problem, we launched a program for observing radio sources at declinations [-90°, -40°] with Long Baseline Array (LBA) in 2008. The main goal of the program was to increase the density of calibrator sources with positions known at milliarcsecond level in the southern hemisphere to make an analogue of VCS in the south. Unlike to the VCS surveys at the northern hemisphere, we used predominately AT20G at 20 GHz from Australia Telescope Compact Array (ATCA) observations for drawing the candidate list for LBA observations.

The results of the first part of this campaign for observing the brightest sources, the catalogue LCS–1 was published by (Petrov et al. 2011b). Here we present results of the second, final part of the campaign. In the following sections we describe observations, data analysis, analysis of errors, and investigate the relationship of the correlated flux density at milliarcsecond scales derived from our VLBI observations with flux densities of the parent AT20G catalogues at arcseconds scales.

2 OBSERVATIONS

2.1 Network

The network of observing station includes 11 stations listed in Table 1, although at any given experiment only a subset of stations participated. The list of VLBI experiments, observation dates, and the participating network is shown in Table 2. The network, except station Hh, is shown in Figure 1. Station As participated in three experiments, station Td observed only during 4–8 hours intervals. The 64 m station Pa was scheduled in every experiment, in every scan of target sources since it is the most sensitive station of the network and the baselines with Pa are the most sensitive.

Stations At, Mp and Cd were equipped with the LBA VLBI backend consisting of an Australia Telescope National Facility (ATNF) Data Acquisition System (DAS) with an

Table 1. The LBA network. The typical System Equivalent Flux Density (SEFD) at 8.3 GHz at elevation angles > 45° achieved in LCS experiments **is shown** in the last column.

Code	Name	ϕ_{gc}	λ	Diam	SEFD
As	ASKAP	-26°.53	116°.63	12 m	8300 Jy
At	ATCA	-30°.15	149°.57	5 × 22 m	140 Jy
Cd	CEDUNA	-31°.70	133°.81	32 m	600 Jy
Ha	HARTRAO	-25°.74	27°.69	26 m	1200 Jy
Ho	HOBART26	-42°.62	147°.44	26 m	850 Jy
Ke	KATH12M	-14°.28	132°.15	12 m	3000 Jy
Mp	MOPRA	-31°.10	149°.10	22 m	400 Jy
Pa	PARKES	-32°.82	148°.26	64 m	50 Jy
Td	TIDBINBILLA	-35°.22	148°.98	34 m	120 Jy
Yg	YARRA12M	-28°.88	115°.35	12 m	3000 Jy
Ww	WARK12M	-36°.25	174°.66	12 m	3000 Jy

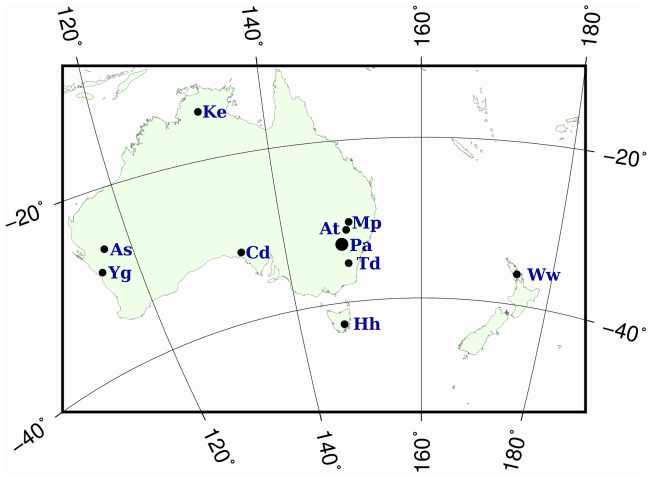

Figure 1. The LBA stations network. Station Hh (HARTRAO), 60 km north-west of Johannesburg, South Africa, is not shown.

LBADR recorder. The ATNF DAS only allows two simultaneous intermediate frequencies (IFs): either 2 frequencies or 2 polarizations. For each of these IFs the input 64 MHz analog IF is digitally filtered to 2 contiguous 16 MHz bands. Stations At and Mp were equopped with two LBDAR recorders, howerever additional recorders could not be used for expanding the bandwidth due to hardware limitations, but could be used for recording both polarizations. Thus, the stations equipped with the ATNF backend could record two bands 32 MHz wide. This imposed a limitation on the frequency setup: spreading the frequencies too narrow would result in degradation of group delay accuracy and spreading the frequencies two wide would results in group delay ambiguities with very narrow group delay ambiguities spacings. Our choice was to spread 32 MHz sub-bands at 256 MHz that allowed to determine group delay with uncertainly 123 ps when the signal to noise ratio is 10 and with ambiguity 3.9125 ns.

Other stations were equipped with Mark-4 data acquisition terminals that were replaced with Mark-5 during to the course of the campaign. Station Cd was upgraded from the ATNF backend to Mark-5 in 2015 and used Mark-5 in last three campaigns. Stations equipped with Mark-5 recorded

Table 2. List of the LBA Calibrator Survey experiments. The first column shows the campaign segment, the second and third show the observing session and experiment ID, and the last segment shows the network of participating stations.

LCS–1	20080205_r	v254b	At-Cd-Ho-Mp-Pa
LCS–1	20080810_r	v271a	At-Cd-Ho-Mp-Pa-Td
LCS–1	20081128_r	v271b	At-Cd-Ho-Mp-Pa-Td
LCS–1	20090704_r	v271c	At-Cd-Ho-Mp-Pa
LCS–2	20091212_r	v271d	At-Cd-Ho-Mp-Pa
LCS–2	20100311_r	v271e	At-Cd-Ho-Mp-Pa
LCS–2	20100725_p	v271f	At-Cd-Ho-Mp-Pa
LCS–2	20101029_p	v271g	At-Cd-Mp-Pa
LCS–2	20110402_p	v271h	At-Cd-Ho-Hh-Ww-Td
LCS–2	20110723_p	v271i	As-At-Cd-Ho-Hh-Mp-Pa-Td-Ww
LCS–2	20111111_p	v271j	At-Cd-Ho-Hh-Mp-Td
LCS–2	20111112_p	v441a	At-Cd-Ho-Hh-Mp-Td
LCS–2	20120428_p	v271k	At-Cd-Ho-Hh-Mp-Pa-Ww-Yg
LCS–2	20130315_p	v271l	As-At-Cd-Ho-Hh-Mp-Pa-Ww-Td
LCS–2	20130615_p	v271m	At-Cd-Ho-Hh-Mp-Pa-Ww-Td
LCS–2	20140603_p	v493a	At-Cd-Ho-Hh-Mp-Pa-Td
LCS–2	20150407_p	v271n	At-Cd-Ho-Hh-Ke-Pa-Ww-Yg
LCS–2	20150929_q	v271o	As-At-Cd-Ho-Hh-Ke-Pa-Ww-Yg
LCS–2	20160628_q	v493c	As-At-Cd-Ke-Mp-Pa-Yg

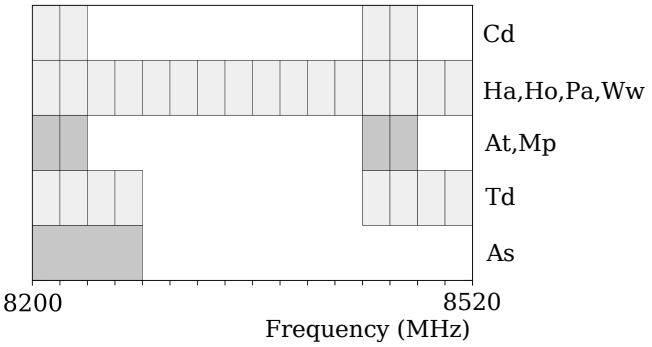

Figure 2. The frequency allocation in v271i experiment. The channel width is 16 MHz for all stations, except As, which has the channel width 64 MHz. Single polarization channels are shown with light-gray color and dual polarization channels are shown with dark-Gray color.

256 MHz bandwidth, except Td that prior 2016 was able to record only 128 MHz and station As that could record a single bandwidth 64 MHz, dual polarization. Stations equipped with Mark-4 or Mark-5 recorded more 16 MHz wide frequency channels with 320 MHz wide bandwidth that partly overlapped with the frequency channels recorded by the stations with the ATNF backend In every experiment network stations used from 2 to 5 different setups and these setups were changing from the experiment to experiment. Figure 2 shows as an example the frequency setup of v271i experiment. The versatility of the DiFX-2 correlator (Deller et al. 2011) allowed to cross-correlate the overlapping regions of such experiments. The heterogeneity of the the available VLBI hardware made correlation more difficult but, fortunately did not introduced noticeable systematic errors in group delay. The most profound effect of this frequency allocation is ambiguities in group delay at baselines with stations that record with the ATNF backend.

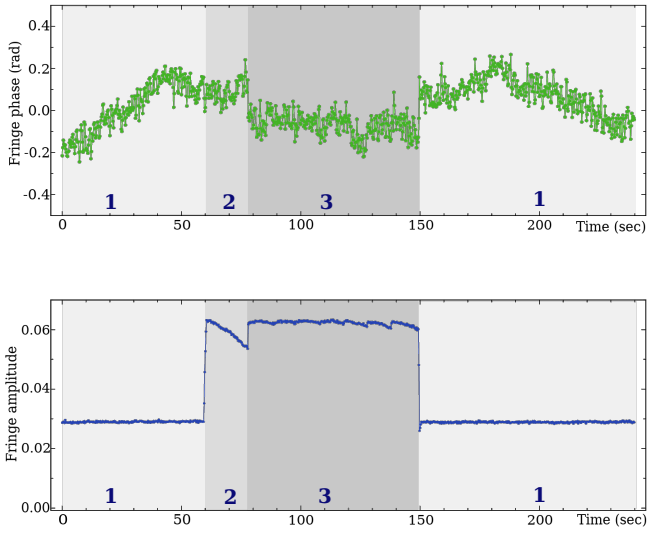

Figure 3. The fringe plot at ATCA/PARKES, source J2225-0457 during vt10k test experiment. The upper plot shows fringe phase, the lower plot shows fringe amplitude. Light-gray area "1" denotes the interval when single ATCA station records. The dark-gray area "3" denotes the interval when the phased-array records. The medium-gray area "2" denotes the intermediate interval.

The Australia Telescope Compact Array (ATCA) consists of six 22 m antennas. Five of them can be phased up and record signal as a single element of the VLBI network. The position of the ATCA phase center can be specified by the user. This feature became available in 2009 **Chris, correct?**. However, we exercised a caution in using phased ATCA since attempts to use phased Westerbork array for astrometry revealed significant phase fluctuations which rendered it highly problematic for precise astrometry (Pogrebenko, private communication, 2010). Therefore, we investigated performance of phase ATCA in a special 4 hour long test experiment that we ran on May 08, 2010. Stations ATCA, CEDUNA, HOBART26, MOPRA, and PARKES recorded the same frequency setup as in the LCS experiments. For the first 60 seconds of a 4 minute long scan ATCA recorded signal from the single antenna at pad with ID 104 (see LCS1 paper for the nomenclature of ATCA pads), then it switched to the phased array with the phase center at the same pad and recorded for 90 second. Finally, it ATCA switched back to recording the signal from a single station. In total, 232 scans of strong sources were recorded. The typical plots of the normalized uncalibrated fringe amplitude and fringe phase as a function of time within a scan are shown in figure 3. Corr 1

We see that for 18 seconds after switching to the phased-up mode the fringe amplitude is steadily drops by 15stable within 2%. We consider this as transitional interval. **Chris, we need to explain this behavior**. The fringe phase does not show change greater 0.01 rad just after switching back to the phased mode, but shows a sudden change in a range of 0.1–0.2 rad after the end of the transitional interval and immediately after switching from the phased to the single antenna record mode. Corr 2

We computed average fringe phases, phase delay rates, group delays and group delay rates by running the fringe fitting algorithm trough the same data three times. During the

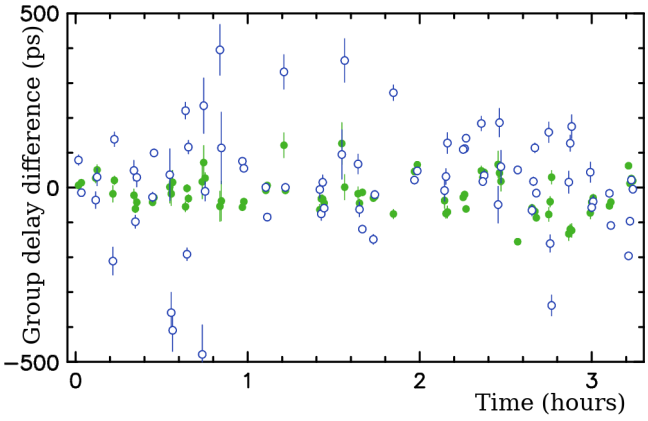

Figure 4. Differences in group delays from the same observations in test vt10k experiment. The solid green circles show the differences in group delay between ATCA phased-array and ATCA-single stations. The wrms of the differences is 38 ps. For comparison, the whole blue circles show the differences in group delay from first 60 sec and last 90 seconds of the integration interval.

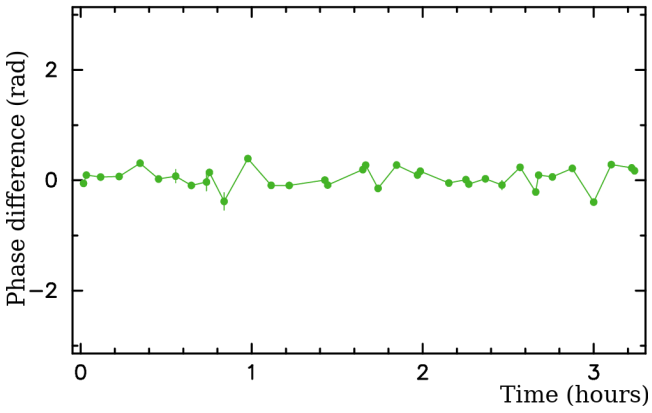

Figure 5. Differences in fringe phase delays between ATCA phased-array and ATCA-single recording from the same observations in test vt10k experiment. The wrms of the differences ins 0.12 rad.

first processing run we masked out single antenna recording mode and the first 18 s of the phased recording mode keeping 72 s long data in each scan when ATCA recorded in the phased mode. During the second processing run we masked out the data when ATCA recorded in the phased mode. During the third run we processed first 60 s and last 90 s of each scan when ATCA recorded in the single antenna mode. We referred group delay and fringe phases to the same common epoch within a scan and formed their differences.

The differences in group delay between phased and single antenna recording mode at different baselines with ATCA is shown on Figure 4 with green color. The wrms of the differences is 38 ps. For comparison, the differences in group delays computed using the first 60 seconds and last 90 seconds of a 4 minute long scan recorded at ATCA in the single antenna mode and referred to the same middle epoch are shown with blue color. The wrms of these differences is 59 ps. The differences in fringe phase between recording at ATCA with phased model and single antenna mode are shown in Figure 5. The wrms of phase differences is 0.12 rad.

We analyzed dependence if the differences versus elevation, azimuth and parallactic angle, but found no pattern. The uncalibrated averaged fringe amplitude at baselines with ATCA data recorded as a phased array is a factor of 2.27 greater than the uncalibrated fringe amplitude with ATCA data recorded as a single antenna, which is within 2% of $\sqrt{5}$.

We conclude that phasing ATCA up does not introduce noticeable systematic errors in group delay and fringe phases. The differences in group delays is a factor of 1.5 less than the difference in group delay computed from two subset of data separated by 90 s. The differences in phases is random noise with wrms is 0.12 rad, which corresponds to 0.6 mm. Therefore, we concluded that using of phased ATCA as an element of the VLBI network does not introduce systematic errors, but improves sensitivity of ATCA by a factor of 2.27. This was the first use of phased array as an element of VLBI network for absolute astrometry.

2.2 Source selection

We selected for observations the target sources that were previously detected with single dish observations or with connected interferometers at baseline 0.1–5 km. The input catalogues provided the estimates of flux density at resolutions 1–100″. The response of an interferometer to an extended source depends on its compactness and the size of the interferometer. The baseline projection lengths of the LCS network vary in a range of 5–300 Mλ. That means the interferometer will be sensitive for emission from the compact components of milliarcsecond size. The response to extended emission with a size more than 1 mas at the longest baselines and 50 mas at the shortest baselines will be attenuated, and the interferometer will not detect signal from emission with size a more than a factor 2–5 beyond that level.

In order to maximize the number of detected sources, we have to select the targets with the highest compactness: the ratio of the correlated flux density at 5–300 Mλ to the total flux density. As a marker of high compactness we initially used spectral index defined as $S \sim f^{\alpha}$, where f is the frequency. As a result of synchrotron self-absorption the emission from the optically thick jet based that is morphologically referred to as the core of an AGN, has flat ($\alpha \approx 0$) or inverted spectrum ($\alpha > 0$). The optically think emission from the extended jet and extended radio-lobes that are a result of interaction of the jet with surrounding interstellar medium usually has steep spectrum ($\alpha < 1$). Therefore, one can expect the sources with flat spectrum, on average, will have a higher compactness, which was confirmed with observations (e.g., Beasley et al. 2002).

For the coarse of the 8-year long campaign our sources selection strategy gradually evolved, but all the time it was focused on selecting the sources with brightest correlated flux density. In the first three experiments we selected the sources with spectral index > -0.50 from the quarter-Jansky survey (Jackson et al. 2002) brighter 200 mJy. In following experiments were used several criteria for selecting the targets. In experiments v271c–v271m we selected the candidate sources brighter 150 mJy with spectral index > -0.55 from the AT20G catalogue (Murphy et al. 2010). In addition to that, we selected the sources brighter

180 mJy and spectral index > -0.55 from the PMN catalogue (Griffith & Wright 1993; Wright et al. 1994; Griffith et al. 1994; Condon et al. 1993; Tasker et al. 1994; Griffith et al. 1995; Wright et al. 1996). In v271k–v271m experiments we selected the sources brighter 170 mJy and spectral index > -0.55 from the ATPMN catalogue (McConnell et al. 2012).

However, an approach of selecting flat spectrum sources does not provide a good prediction for correlated flux density for the sources within 5–7° of the Galactic plane. First, the the Galactic plane is crowded and a chance to make an error in cross-matching the sources observed with instruments are different resolutions and poor positional accuracy rather high. This will result in a gross mistake in the estimate of the spectral indices. Second, the density of galactic sources with flat spectrum, such as supernova remnants and ultra-compact H II regions is much higher within the Galactic plane. An attempt to observe flat spectrum sources in the Galactic plane by cross-matching the MGPS-2 catalogue at 843 MHz Murphy et al. (2007) resulted in a detection rate of $\sim$10%. To overcome this problem, we used another approach to find candidate sources in the Galactic plane: we analyzed IR color-color diagram. Massaro et al. (2011) noticed that the blazars occupied a special zone in the color-color diagram 3.4–4.6 μm and 4.6–12 μm. We analyzed this dependence independently and delineated the zone that encompasses over 85% compact radio-loud AGNs from the cumulative VLBI catalogue RFC (Petrov & Kovalev, 2017, in preparation[1]). See section 4.2 in Schinzel et al. (2015) for detail. After the failure with cross matching MGPS-2 with higher frequency radio catalogues, we tried the second approach: we selected all the sources within 5° of the Galactic plane and declinations below $-40°$ and flux density > 50 mJy and left those that have cross-matches against IR WISE catalogue (Wright et al. 2010; Mainzer et al. 2011) within $30''$. Then we throw away the sources that are away the zone of the 3.4–4.6 μm and 4.6–12 μm diagram that contains 85% radio loud AGNs. We observed the brightest sources from the remaining sample. The detection rate of this sample was 57%.

In addition to these selection methods, we observed in three experiments, v441a, v493a, and v493c the flat spectrum sources brighter 10 mJy that were detected at 5 and 9 GHz by the Australia Telescope Compact Array (ATCA) within its error ellipse, i.e. 2–5′ of unassociated sources γ-ray sources detected with *Fermi* mission (Abdo et al. 2010) that we found in a dedicated program (Petrov et al. 2013; Schinzel et al. 2015, 2017) focused in finding the most plausible radio counterparts of γ-ray source. Since radio-loud γ-ray AGNs tend to be very compact, the presence of a radio source detected with a connected interferometer within the error ellipse of a γ-ray raises the probability of being detected with VLBI. Observing such sources first, fits the primary goal of the LCS program, second, allows to find an association to *Fermi* objects that previously were considered unassociated.

[1] Preview is available at http://astrogeo.org/rfc

2.3 Scheduling

The experiment scheduled was generated automatically with program sur_sked in a sequence that minimizes the slewing time and obey a number of constraints. Target sources was observed in three-four scans for 2 to 4 minutes long each, except weak targets of candidates to *Fermi* associations that were observe for 5–10 minutes. Observing session had nominal duration of 24 hours. During a session 80–100 target sources were observed. The minimum gap between consecutive observations of the same source was set to 2.5 hours. Station Parkes was required to participate in each scan, since it is the most sensitive antenna of the array. After 1.5 hours of observing targets sources, a block of so-called calibrator sources was inserted. These are the sources picked from the pool of known compact objects stronger 300 mJy. The block consists of 4 sources, with two of them observed at each station in the elevations in the range of 10–30° (30–40° for Parkes that have elevation limit 31°) and two observed at elevations 55–85°. The goal of these observations: 1) to improve the estimate of the atmosphere path delay in zenith direction; 2) to connect the LCS catalogue to the accumulative catalogue of compact radio sources; 3) to use these sources as bandpass calibrator; 4) to use these sources as amplitude calibrators for elevation gain corrections.

3 DATA ANALYSIS

3.1 Correlation and post-correlation analysis

3.2 Astrometric analysis

3.3 Imaging analysis

Alet and Alessandra: here is the place for your song.

3.4 Determination of flux densities

Here I will describe results of non-imaging analysis for those experiments Alet and Alessandra still did not process.

4 ERROR ANALYSIS

5 THE CATALOGUE

6 POPULATION ANALYSIS

Elaine: this is the part where I anticipate your contribution. I suggest to take all the cross-matches between AT20G and VLBI, not limiting ourselves to LCS2 only. The majority of matches will be from LCS1,2 but I do not think we shuld exclude the sources from VLBI.

I bear in mind compactness analysis (ration of VLBI to AT20G flux density), correlation between compactness and spectral indices. Anything else?

7 CONCLUSION

REFERENCES

Abdo A. A., et al., 2010, ApJS, 188, 405

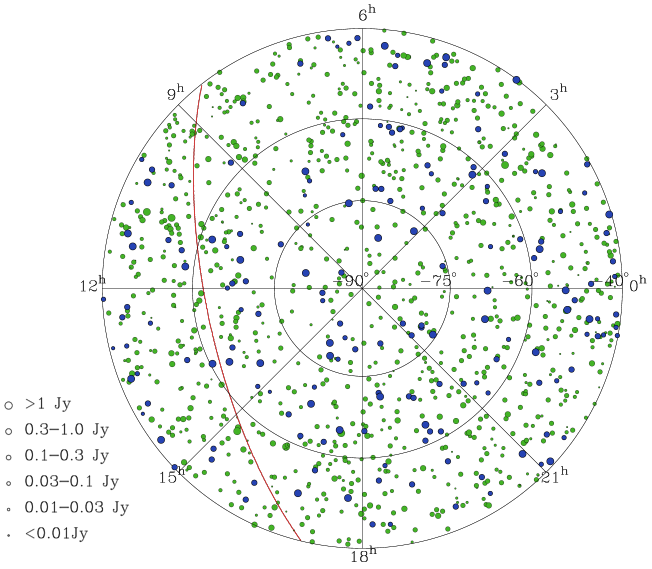

Figure 6. The sky distribution of comact radio source at the southern hemisphere. Blue light color denotes 186 sources with declinations $< -40°$ with VLBI positions known prior the LCS program. Green dark color denotes 1100 sources detected in LCS program. Red line shows the Galactic plane.

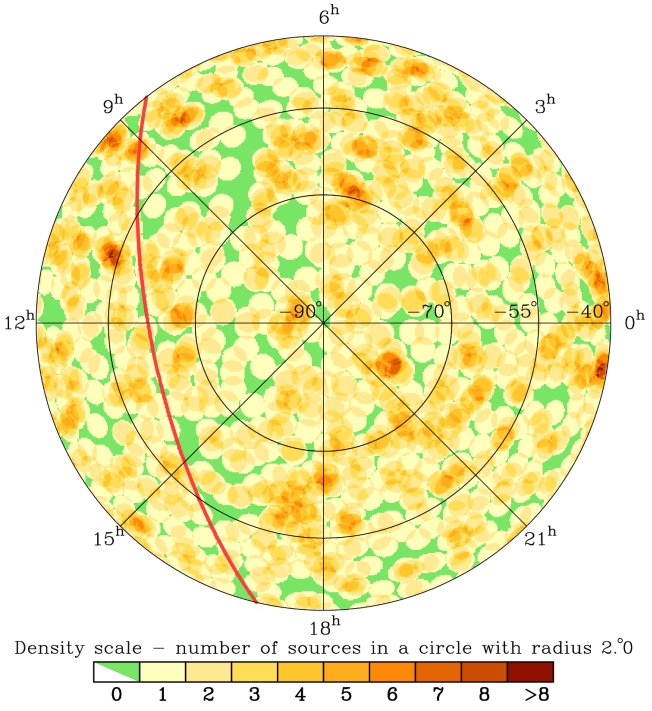

Figure 7. The sky density of calibrator sources in the zone with declinations $< -40°$ defined as the number of compact sources with flux density > 30 mJy in a circle of 2° radious.

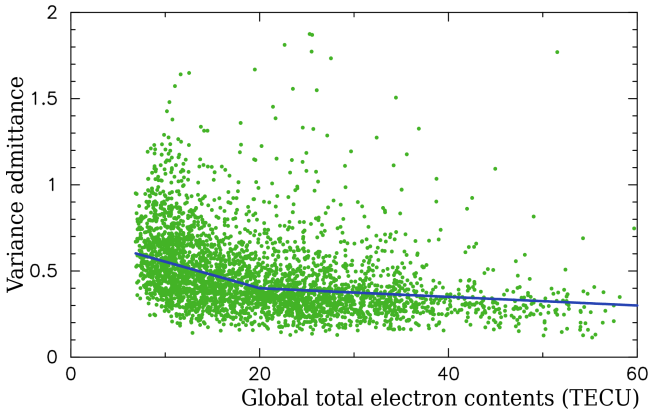

Figure 8. The dependence of the variance admittance factor A on the global total electron contents.

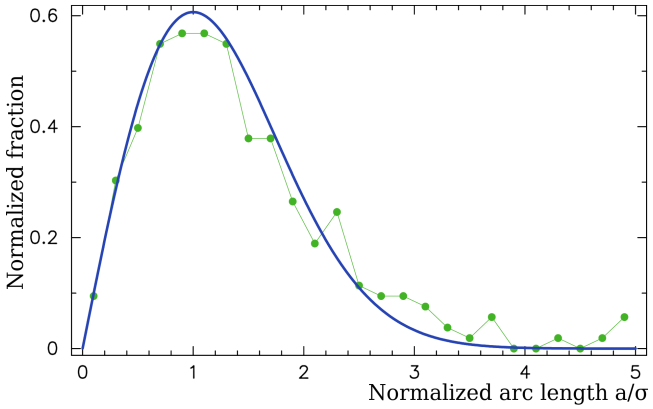

Figure 9. The distribution of the normalized arc lenghts between LCS2 X-band only positions of 269 sources and their X/S positions from the follow-up campaigns (Green dots). For comparision, the Rayleigh distirbution with $\sigma = 1$ parameter is shown with a blue line.

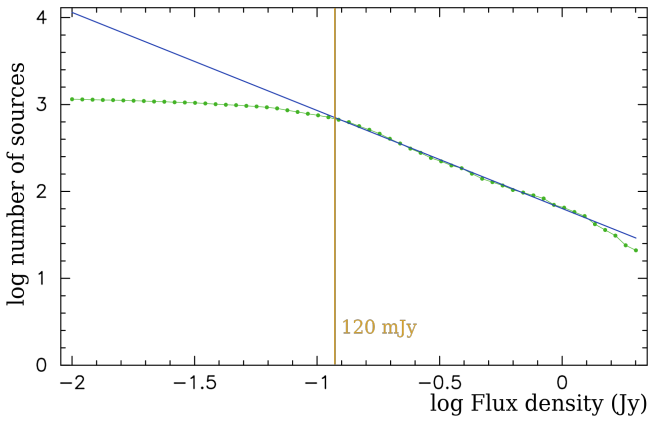

Figure 10. The log N–log S dependence for the LCS2 catalogue.

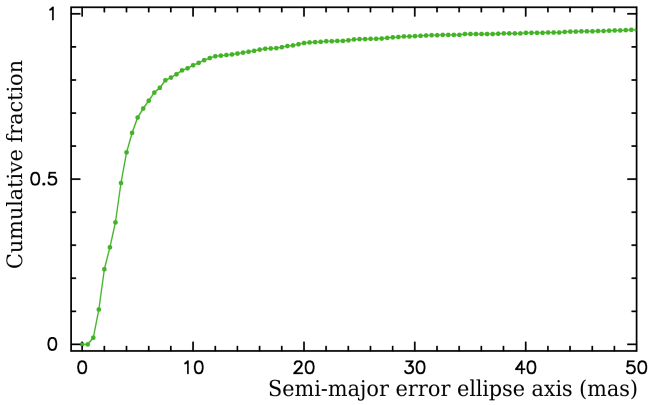

Figure 11. The cumulative distribution of the LCS2 position errors.

Beasley A. J., Gordon D., Peck A. B., Petrov L., MacMillan D. S., Fomalont E. B., Ma C., 2002, ApJS, 141, 13

Condon J. J., Griffith M. R., Wright A. E., 1993, AJ, 106, 1095

Condon J. J., Darling J., Kovalev Y. Y., Petrov L., 2016, preprint, (arXiv:1606.04067)

Deller A. T., et al., 2011, PASP, 123, 275

Fomalont E. B., Petrov L., MacMillan D. S., Gordon D., Ma C., 2003, AJ, 126, 2562

Gordon D., et al., 2016, AJ, 151, 154

Griffith M. R., Wright A. E., 1993, AJ, 105, 1666

Griffith M. R., Wright A. E., Burke B. F., Ekers R. D., 1994, ApJS, 90, 179

Griffith M. R., Wright A. E., Burke B. F., Ekers R. D., 1995, ApJS, 97, 347

Immer K., et al., 2011, ApJS, 194, 25

Jackson C. A., Wall J. V., Shaver P. A., Kellermann K. I., Hook I. M., Hawkins M. R. S., 2002, A&A, 386, 97

Kovalev Y. Y., Petrov L., Fomalont E. B., Gordon D., 2007, AJ, 133, 1236

Kovalev Y. Y., Petrov L., Plavin A. V., 2017, A&A, 598, L1

Lindegren L., et al., 2016, A&A, 595, A4

Mainzer A., et al., 2011, ApJ, 731, 53

Massaro F., D'Abrusco R., Ajello M., Grindlay J. E., Smith H. A., 2011, ApJ, 740, L48

Matveenko L. I., Kardashev N.-S., Sholomitskii G.-B., 1965, Soviet Radiophys., 461, 461

McConnell D., Sadler E. M., Murphy T., Ekers R. D., 2012, MNRAS, 422, 1527

Mignard F., et al., 2016, A&A, 595, A5

Murphy T., Mauch T., Green A., Hunstead R. W., Piestrzynska B., Kels A. P., Sztajer P., 2007, MNRAS, 382, 382

Murphy T., et al., 2010, MNRAS, 402, 2403

Petrov L., 2011, AJ, 142, 105

Petrov L., 2013, AJ, 146, 5

Petrov L., 2016, preprint, (arXiv:1610.04951)

Petrov L., Kovalev Y. Y., 2017a, preprint, (arXiv:1704.07365)

Petrov L., Kovalev Y. Y., 2017b, MNRAS, 467, L71

Petrov L., Taylor G. B., 2011, AJ, 142, 89

Petrov L., Kovalev Y. Y., Fomalont E. B., Gordon D., 2005, AJ, 129, 1163

Petrov L., Kovalev Y. Y., Fomalont E. B., Gordon D., 2006, AJ, 131, 1872

Petrov L., Kovalev Y. Y., Fomalont E. B., Gordon D., 2008, AJ, 136, 580

Petrov L., Kovalev Y. Y., Fomalont E. B., Gordon D., 2011a, AJ, 142, 35

Petrov L., Phillips C., Bertarini A., Murphy T., Sadler E. M., 2011b, MNRAS, 414, 2528

Petrov L., Mahony E. K., Edwards P. G., Sadler E. M., Schinzel F. K., McConnell D., 2013, MNRAS, 432, 1294

Schinzel F. K., Petrov L., Taylor G. B., Mahony E. K., Edwards P. G., Kovalev Y. Y., 2015, ApJS, 217, 4

Schinzel F. K., Petrov L., Taylor G. B., Edwards P. G., 2017, ApJ, 838, 139

Tasker N. J., Condon J. J., Wright A. E., Griffith M. R., 1994, AJ, 107, 2115

Wright A. E., Griffith M. R., Burke B. F., Ekers R. D., 1994, ApJS, 91, 111

Wright A. E., Griffith M. R., Hunt A. J., Troup E., Burke B. F., Ekers R. D., 1996, ApJS, 103, 145

Wright E. L., et al., 2010, AJ, 140, 1868